Hyperfine structure and isotope shift in the $3s^2\,3p^2\,{}^3P_{0,1,2} \rightarrow 3s^2\,3p4p\,{}^3P_{0,1,2}$ transitions in silicon by Doppler-free in-source two-photon resonance-ionization spectroscopy

K. Wendt,[*] C. Mattolat, T. Gottwald, T. Kron, S. Raeder,[†] S. Rothe,[‡] and F. Schwellnus
Institut für Physik, Johannes Gutenberg-Universität Mainz, D-55099 Mainz, Germany

H. Tomita
Department of Quantum Engineering, Graduate School of Engineering, Nagoya University, Nagoya, Aichi 464-8603, Japan
(Received 4 September 2013; published 13 November 2013)

A high-resolution technique for direct in-source laser spectroscopy within a hot cavity laser ion source has been demonstrated by applying Doppler free two-photon resonance ionization spectroscopy. An injection-locked narrow-bandwidth pulsed titanium:sapphire laser operating in high repetition rate was used for resonance ionization of silicon. The isotope shift of ^{28}Si, ^{29}Si, and ^{30}Si as well as the hyperfine structure of all two-photon transitions of the $3s^2\,3p^2\,{}^3P_{0,1,2} \rightarrow 3s^2\,3p4p\,{}^3P_{0,1,2}$ multiplet for ^{29}Si were recorded at an overall experimental spectral linewidth of 90 MHz.

DOI: 10.1103/PhysRevA.88.052510 PACS number(s): 32.30.−r, 32.80.Rm, 42.55.Rz, 42.60.Fc

I. INTRODUCTION

On-line isotope separators like the Isotope Separator On-Line DEvice (ISOLDE) at CERN, Geneva; the Isotope Separator and Accelerator at TRIUMF, Vancouver; and a few others worldwide give favorable access to exotic short-lived isotope far-off stability as well as to those all-radioactive elements that exhibit only short-lived isotopes like astatine [1–3]. In-source laser resonance ionization today is the method of choice for production of pure ion beams at these radioactive ion-beam facilities [4,5]. It significantly suppresses the major limitation for any subsequent laser or nuclear spectroscopic investigation, which is caused by contaminations of isobars and neighboring isotopes in the extracted, mass-separated ion beam. In addition, the technique could serve for direct medium- or even high-resolution laser spectroscopic studies on exotic radio isotopes by efficiently avoiding decay losses. Nevertheless, up to now the approach of laser spectroscopy directly inside the ion source of the mass separator suffers from the large Doppler broadening of the optical resonance lines. The latter is unavoidable due to the hot cavity ion source environment that is required to ensure efficient and fast release of short-lived exotic species after production in the nearby nuclear reaction target [6–9]. Thus, so far only medium-resolution in-source spectroscopy with linewidths in the GHz range has been demonstrated, which nevertheless enabled isomer selection [10]. A promising approach to overcome these limitations toward high-resolution in-source laser spectroscopy is the application of Doppler free two-photon spectroscopy in combination with subsequent efficient resonance ionization using narrow-bandwidth, high-power laser systems. To meet both requirements mandatory for operation at on-line facilities, i.e., high laser power and narrow spectral bandwidth, a dedicated injection-locked pulsed Ti:sapphire laser was developed and applied in this study. It operates at high repetition rate and offers average output power above 1 W at a spectral bandwidth of about 20 MHz. The general feasibility of Doppler free two-photon resonance ionization spectroscopy inside the typical hot ion source cavity of an online isotope separator and the suitability of the newly developed laser system are demonstrated. Measurements were carried out at the so-called Mainz University atomic beam unit (MABU), described below, aiming for resolution of hyperfine structure (HFS) and isotope shift in the spectrum of the so far only purely investigated element silicon. The isotope shift between all three stable silicon isotopes ^{28}Si, ^{29}Si, and ^{30}Si, out of which both ^{29}Si and ^{30}Si have rather low natural abundances (<5%), was successfully measured in the $3s^2 3p^2\,{}^3P_0 \rightarrow 3s^2 3p4p\,{}^3P_0$ two-photon transition. For the odd-A isotope ^{29}Si with nuclear spin $I = 1/2$, in addition, the hyper-fine-structure splittings in all permitted two-photon transitions between the $3s^2 3p^2\,{}^3P_{0,1,2}$ ground state and the $3s^2 3p4p\,{}^3P_{0,1,2}$ excited state fine-structure multiplets could be resolved. Applying the well-developed theory for two-photon transitions, the hyperfine A factors could be extracted for all members of the ground- and excited-state multiplets. We shall first present the spectroscopic situation in Si I and the experimental arrangement used in our study. Afterward, the necessary theoretical background for proper analysis of the two-photon hyperfine spectra is introduced briefly, while the following section discusses the measured results in comparison to the few existing earlier data.

II. SPECTROSCOPIC BACKGROUND IN SILICON

Due to the high evaporation temperature and unpleasant wavelength of ground-state resonance lines of silicon in the ultraviolet spectral region well below 300 nm, optical high-resolution spectroscopic investigations on this element are rare. Nevertheless, detailed spectroscopic knowledge on the overall level scheme exists of Si I with a multitude of highly excited states known, almost exclusively belonging to atomic configurations with a core of $3s^2 3p$ and one excited valence electron with angular momentum L in the range of

[*]klaus.wendt@uni-mainz.de; http://www.larissa.physik.uni-mainz.de
[†]Present address: Instituut voor Kern- en Stralingsfysica, KU Leuven, B-3001 Leuven, Belgium.
[‡]Present address: ISOLDE, CERN, Geneva, Switzerland.

 ©2013 American Physical Society

$L = 1$ to 3. Only two bound configurations with a breakup of the $3s^2$ system in the leading term have been reported so far, $3s3p^3\,{}^5S^o_2$ and $3s3p^3\,{}^3D^o_J$, located energetically at 33 326 and around 45 000 cm^{-1}, respectively. In contrast, two different $3s^23pnd$ Rydberg series have been studied in great detail up to principal quantum number $n = 56$, delivering the ionization potential (IP) of 65 747.76 cm^{-1} as well as the second low-lying state to higher angular momentum J of the singly charged ion [11]. The isotope shift between ^{28}Si and ^{30}Si was investigated as early as 1961 by Holmes and Hoover [12] using classical spectroscopy in a cooled hollow discharge and addressing a number of resonance and intercombination lines in the spectral range of 210–290 nm. In the field of laser spectroscopy within the atomic spectrum of silicon, only a few studies mainly devoted to trace analytical purposes have been reported. These applied sputter initiated resonance ionization spectroscopy, utilizing one of the strong $3s^23p^2\,{}^3P_{0,1,2} \rightarrow 3s^23p4s\,{}^3P^o_{0,1,2}$ transitions together with immediate nonresonant ionization or alternatively involving a second intermediate resonant excitation step. Recently and in parallel to our study, Lee and Fairbank, Jr. carried out high-resolution studies in the $3s^23p^2\,{}^3P_2 \rightarrow 3s3p^3\,{}^3D^o_3$ at 221.7 nm in preparation of a silicon-atom-based quantum computer, which delivered isotope shift values for all stable isotopes ^{28}Si, ^{29}Si, and ^{30}Si as well as hyper-fine-structure A factors for ^{29}Si in the $3s^23p^2\,{}^3P_2$ ground state and the $3s3p^3\,{}^3D^o_3$ excited state [13]. Due to the nuclear spin of $I = \frac{1}{2}$ no electric quadrupole interaction occurs and the magnetic dipole interaction is simply given by

$$\Delta\nu_{\mathrm{HFS}} = \frac{AC}{2}, \tag{1}$$

where the A factor is proportional to the nuclear dipole moment $A = \mu_I B_J$ and $C = [F(F+1) - I(I+1) - J(J+1)]$ is the Casimir factor.

The isotope shift in this light mass region is strongly dominated by the mass effect, which is caused by the reduced mass correction (normal mass shift) and the influence of correlations in the motion of the different electrons (specific mass effect). The second term is theoretically accessible only by extensive computer calculations and in most cases nevertheless not precisely quantifiable. Nevertheless, in all cases a direct proportionality of the mass shift to the mass difference is found. A second contribution to the isotope shift, stemming from the variation of the nuclear size and the resulting field distribution between neighboring isotopes (field effect) is comparably small for light masses. Correspondingly, a rather similar shift between neighboring isotopes is expected here, with its size dominantly depending on the transition wavelength and the angular momentum J of the levels involved.

III. EXPERIMENTAL SETUP

A. Laser setup

A laser suitable for combination of Doppler free two-photon spectroscopy and efficient resonance ionization inside a hot cavity must meet several challenging requirements: Integration into the existing laser setups typically used at resonance ionization laser ion sources (RILISs) requires pulsed operation with a repetition rate of about 10 kHz, pulse durations of 30 ns or below, and average output power on the order of up to several watts. The solid-state laser systems, which nowadays are in use at the leading ISOL facilities worldwide, e.g., ISOLDE-RILIS at CERN in Geneva, Switzerland and TRIUMF's TRILIS in Vancouver, Canada, utilize up to three Ti:sapphire lasers, which operate well synchronized by intracavity Q switching. For each laser an intracavity birefringent filter and etalon serve as frequency selective elements, which produce a spectral bandwidth of typically 3 GHz [14]. This value perfectly matches the Doppler profile of the atomic ensemble in the hot cavity source but so far prevented any application for high-resolution approaches like two-photon spectroscopy, which would require a laser bandwidth well below 100 MHz. This specification has been realized in this work by injection locking of a pulsed high repetition rate Ti:sapphire laser onto the narrow-bandwidth radiation from a continuous-wave external-cavity diode laser (ECDL), which acted as a master oscillator. This laser was used for both efficient two-photon excitation between bound states in Si I as well as nonresonant ionization above the first ionization potential via absorption of a third photon. The layout of the injection-locked laser system is schematically shown on the right side in Fig. 1.

To ensure operation on a single longitudinal mode the usual Z-shaped standing-wave resonator of the Ti:sapphire laser was converted into a bow-tie shaped ring laser cavity, keeping all resonator dimensions as identical as possible. For protection of the sensible laser diodes of the master laser against the intense Ti:sapphire laser pulses, three consecutive optical isolators with a suppression of 160 dB in total were used. After spatial mode matching, the beam of the ECDL is injected as seed into the cavity of the Ti:sapphire laser, which simultaneously is pumped by a frequency doubled Nd:YAG laser at 532 nm. The ring resonator cavity length was actively stabilized by a dither-lock technique with a modulation width of about 20 MHz, which dominates the finally achieved spectral bandwidths of the pulsed laser radiation slightly above the Fourier limit of about 10 MHz for a 50-ns laser pulse. The intense energy

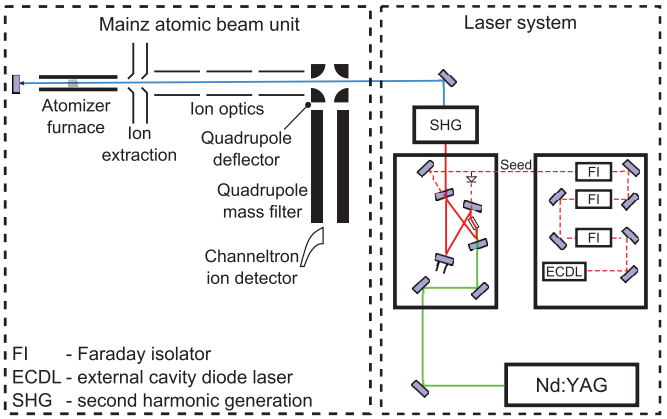

FIG. 1. (Color online) Sketch of the experimental setup showing the mass spectrometer unit MABU as well as the injection-locked Ti:sapphire laser system. The narrow-bandwidth, low-power laser radiation of the ECDL is used for the injection locking of the Ti:sapphire laser. After SHG the light is sent into the ion source cavity of the MABU mass spectrometer. For the two-photon excitation the hot cavity furnace is open at both ends and the laser radiation is reflected back after transmission. More details are described in the text.

within each laser pulse required active electronic blanking of the detecting photodiode and the amplifying electronics of the amplification circuitry during arrival of each pump pulse. Fast signal processing was carried out in between consecutive pulses for resonator stabilization and length control. A detailed description of the laser layout and the stabilization technique has been given in [15,16]. The measurements were carried out at a slightly reduced repetition rate of 7 kHz and with an average pumping power of 15 W per Ti:sapphire laser. Up to 2.5 W of tunable laser light with a pulse duration of 50 ns was generated. The spectral bandwidth of about 20(5) MHz was determined within a 300-MHz scanning Fabry-Perot etalon used as a spectrum analyzer.

For two-photon spectroscopy in silicon an antireflection coated laser diode was used in the ECDL which could be tuned for emission from 790 to 860 nm at a maximum output power of 70 mW. The master laser was set to the required wavelengths of the Ti:sapphire fundamental output between 813 and 819.5 nm to access all possible two-photon transitions between the $3s^2 3p^2\ ^3P_{0,1,2}$ ground-state and the $3s^2 3p 4p\ ^3P_{0,1,2}$ excited-state HFS multiplets. During the measurements the injection-locked laser operated at a power of about 2 W, which resulted in about 130 mW frequency doubled laser light obtained in single pass transmission through a beta barium borate crystal. This radiation was used to drive the two-photon transitions as well as for nonresonant ionization from the excited levels for subsequent efficient ion detection.

B. Hot cavity design for two-photon spectroscopy and mass separator adaptation

The spectroscopic investigations on Si were performed within a dedicated hot cavity RILIS ion source arrangement installed at the Mainz atomic beam unit (MABU). For efficient atomization of silicon a graphite tube with an inner diameter of 2.2 mm and a length of 50 mm was resistively heated to temperatures up to 2300 K. In order to perform two-photon spectroscopy the tube was open on both ends. The laser beam was aligned anticollinearly to the extracted ion beam on the tube axis and was retroreflected backward by a mirror installed behind a window outside the vacuum chamber. Figure 1 shows a sketch of the setup. Silicon was introduced into the graphite tube as nitrate on a titanium foil, which enhances reduction of the oxidic form. Ions created inside the hot cavity by the laser light were pulled toward the front exit hole by the gradient of the heating potential and were extracted by a static electric acceleration field of about 100 V. Ion beam forming was achieved immediately downstream by an einzel lens. A 90° static quadrupole deflector served for separation of the low-energy ion beam from any effusing neutral particles on the axis of the entering laser beam. It directed the ions into a quadrupole mass filter for mass selection and final ion detection by a channeltron detector. The laser beam was focused with a telescope into the middle of the hot graphite tube. Due to a very long focal length chosen and the short distance between the hot cavity and the retroreflecting mirror, a plane mirror could be used for the back reflection of the laser light, strongly simplifying optical alignment.

IV. THEORETICAL BACKGROUND OF TWO-PHOTON EXCITATION

A. Two-photon transition probability

The general theory of multiphoton transitions without a real intermediate state was developed as early as 1931 by Goeppert-Mayer on the basis of applying perturbation theory up to second order [17]. The particular line shape of a two-photon transition induced by a standing electromagnetic wave, as, e.g., generated by retroreflecting a laser beam into itself, leads to complete suppression of the Doppler broadening and a resulting experimental width of two-photon resonances in the same order as the natural linewidth. Vasilenko, Chebotaev, and Shishaev were the first to notice this effect, which led to numerous applications of the technique for high-resolution studies, concerning, e.g., investigations of narrow fine and hyperfine structures or isotope shifts [18]. A detailed review on the topic is given by Grynberg and Cagnac, which covers also the tensorial formalism of two-photon spectroscopy required to understand intensities of fine- and hyperfine-structure components [19]. Here we shall closely follow their notation for analyzing transition probabilities, selection rules, and hyperfine component intensities of the two-photon process studied in silicon.

The Doppler free two-photon transition probability for a transition from a state α (e.g., the ground state) to a state β (e.g., an excited state) induced by a standing electromagnetic wave is given in second-order perturbation theory by summation over all possible intermediate states accessible via electric dipolar radiation as

$$P^{(2)}_{\alpha\beta}(\delta\omega) = \left| \sum_i \frac{\langle \beta\,|\mathcal{H}_1|\,i\rangle\langle i|\mathcal{H}_2|\alpha\rangle + \langle\beta|\mathcal{H}_2|i\rangle\langle i|\mathcal{H}_1|\alpha\rangle}{\Delta\omega_i} \right|^2 \times \frac{\Gamma_\beta}{4\delta\omega^2 + \frac{1}{4}\Gamma_\beta^2}. \quad (2)$$

The variables included here are (1) $[\mathcal{H}_1,\mathcal{H}_2]$—the Hamiltonians of electric dipole interaction between the incident and reflected wave and the atom; (2) $[\Delta\omega_i]$—the deviation of the laser frequency from a single-photon transition to an intermediate state i; (3) $[\Gamma_\beta]$—the natural linewidth of the excited level; and (4) $[\delta\omega]$—the deviation of the laser frequency from the resonance frequency of the two-photon transition of $\omega = \frac{1}{2\hbar}\langle E_\beta - E_\alpha\rangle$, with E_α and E_β being the level energies.

The last term of the equation marks the Lorentzian shape and width of the resonance. Note that due to the odd character of the dipole operator the states α and β must have the same parity, while all the states i must have the opposite parity.

In the case of resonance $\langle\delta\omega = 0\rangle$ and equal laser intensities $\mathcal{H} = \mathcal{H}_1 = \mathcal{H}_2$ the equation strongly simplifies to the tensorial form as given by

$$P^{(2)}_{\alpha\beta}(0) = \left| \sum_i \frac{\langle \beta\,|\mathcal{H}|\,i\rangle\langle i|\mathcal{H}|\alpha\rangle}{\Delta\omega_i} \right|^2 \times \frac{16}{\Gamma_\beta}. \quad (3)$$

In the irreducible tensorial set formalism the sum of Hamiltonians may be expressed in the form of

$$P^{(2)}_{\alpha\beta}(0) = \frac{4n^2\omega^2}{\epsilon_0^2\Gamma_\beta}\left|\langle\beta\left|\mathcal{Q}^S_{\epsilon_1\epsilon_2}\right|\alpha\rangle\right|^2, \tag{4}$$

where n describes the number of photons in one of the two identical counterpropagating waves. The two-photon operator $\mathcal{Q}^S_{\epsilon_1\epsilon_2}$ is given by

$$\mathcal{Q}^S_{\epsilon_1\epsilon_2} = \frac{1}{2}\left(\mathcal{D}\epsilon_1\frac{1}{\hbar\omega-\mathcal{H}_0}\mathcal{D}\epsilon_2 + \mathcal{D}\epsilon_2\frac{1}{\hbar\omega-\mathcal{H}_0}\mathcal{D}\epsilon_1\right), \tag{5}$$

with the electric dipole operator $\mathcal{D}$, the polarizations ϵ_i of the two waves, and $\mathcal{H}_0$ being the Hamiltonian of the unperturbed atom for the special case of the ground-state energy set to zero. For excitation with two counterpropagating waves of identical frequency, as it is the case here, the operator $\mathcal{Q}^S_{\epsilon_1\epsilon_2}$ is symmetrical. Due to the additional fact that the dipole operator is coupled twice, its rank is either zero or two, hence representing a superposition of a scalar and a quadrupolar tensor. This knowledge can be applied to calculate selection rules and relative line intensities for the two-photon hyperfine structure.

Using the projection operators $\mathcal{P}(i\,J_i)$ to the subspace $(i\,J_i)$ with i representing either α or β, respectively, as well as the irreducible sets $T^k_q(\alpha J_\alpha,\beta J_\beta)$ as defined initially by Fano in 1957 [20], the operator may be written as

$$\begin{aligned}{}^{\alpha\beta}\mathcal{Q}^S_{\epsilon_1\epsilon_2} &= \mathcal{P}(\alpha J_\alpha)\mathcal{Q}^S_{\epsilon_1\epsilon_2}\mathcal{P}(\beta J_\beta)\\ &= \sum_{k=0,2}\sum_q \frac{\langle\alpha J_\alpha||\mathcal{Q}^k||\beta J_\beta\rangle}{\sqrt{2k+1}}a^k_q(\vec{\epsilon}_1,\vec{\epsilon}_2)T^k_q(\alpha J_\alpha,\beta J_\beta),\end{aligned} \tag{6}$$

with

$$\begin{aligned}T^k_q(\alpha J_\alpha,\beta J_\beta) = \sum_{m_\alpha m_\beta}(-1)^{J_\beta-m_\beta}\langle J_\alpha J_\beta m_\alpha,-m_\beta|kq\rangle\\ \times|\alpha J_\alpha m_\alpha\rangle\langle\beta J_\beta m_\beta|,\end{aligned} \tag{7}$$

where $\langle J_\alpha J_\beta m_\alpha,-m_\beta|kq\rangle$ is the corresponding Clebsch-Gordan coefficient.

The coefficients $a^k_q(\vec{\epsilon}_1,\vec{\epsilon}_2)$ in general are functions of the polarizations of the laser beams. In the simple case of counterpropagating beams with standard polarization they are just given by Clebsch-Gordan coefficients, i.e.,

$$a^k_q(\epsilon_1,\epsilon_2) = \tfrac{1}{2}[\langle kq|11\epsilon_1\epsilon_2\rangle + \langle kq|11\epsilon_2\epsilon_1\rangle]. \tag{8}$$

Selection rules for the electronic angular momenta J of ground and excited states are introduced by using the Wigner-Eckart theorem on ${}^{\alpha\beta}\mathcal{Q}^S_{\epsilon_1\epsilon_2}$: $|J_\alpha - J_\beta| \leqslant 2$, with $J_\beta = 1 \to J_\alpha = 0$ as well as $J_\beta = 0 \to J_\alpha = 1$ being forbidden.

These selection rules for J are also valid for the total angular momenta F generated by vector coupling of J to the nuclear spin I. In specific cases even more precise rules for F may hold valid, as explored in [21].

B. Hyperfine structures and line intensities

As discussed above, the two-photon tensor operator ${}^{\alpha\beta}\mathcal{Q}^S_{\epsilon_1\epsilon_2}$ in most cases combines contributions of a scalar and a quadrupolar operator. To determine line intensities for the permitted two-photon HFS components for the transitions studied in ^{29}Si, three classes must be considered:

(1) If $J_\alpha \neq J_\beta$, ${}^{\alpha\beta}\mathcal{Q}^S_{\epsilon_1\epsilon_2}$ is purely a quadrupolar operator.

(2) If $J_\alpha = J_\beta = J$ and $J \geqslant 1$, the operator ${}^{\alpha\beta}\mathcal{Q}^S_{\epsilon_1\epsilon_2}$ is a superposition of a scalar and quadrupolar contribution with a ratio depending on the individual F values and the beam polarizations.

(3) If $J_\alpha = J_\beta = J = 0$ or $1/2$, ${}^{\alpha\beta}\mathcal{Q}^S_{\epsilon_1\epsilon_2}$ is purely scalar and obviously only one HFS component is present.

The relative line intensities of the individual HFS components may be derived by

$$\begin{aligned}I_{\alpha\beta}(F_\alpha,F_\beta) &\propto (2F_\alpha+1)\\ &\times\left[R(\alpha,\beta)\delta_{F_\alpha F_\beta} + (2F_\beta+1)\begin{Bmatrix}J_\alpha & J_\beta & 2\\ F_\beta & F_\alpha & I\end{Bmatrix}^2\right],\end{aligned} \tag{9}$$

using Wigner $6j$ symbols. Here $R(\alpha,\beta)$ is the ratio of the reduced matrix elements of the pure scalar operator $\mathcal{Q}^0$ to the pure quadrupole operator $\mathcal{Q}^2$, given by

$$R(\alpha,\beta) = \frac{\langle\alpha J_\alpha||\mathcal{Q}^0||\beta J_\beta\rangle^2}{\frac{1}{5}\langle\alpha J_\alpha||\mathcal{Q}^2||\beta J_\beta\rangle^2}. \tag{10}$$

It is vanishing for the first class where ${}^{\alpha\beta}\mathcal{Q}^S_{\epsilon_1\epsilon_2}$ is purely quadrupolar. Under the assumption that the two-photon transition probability is strongly dominated by the contribution of only one particular intermediate state with J_r, for which it is much larger than for all the other intermediate states, $R(\alpha,\beta;J_r)$ may be computed numerically according to

$$R(\alpha,\beta;J_r) \cong \left[3(2J_\alpha+1)\begin{Bmatrix}J_\beta & J_\alpha & 2\\ 1 & 1 & J_r\end{Bmatrix}^2\right]^{-1}. \tag{11}$$

Although the approximation is rather poor for most realistic cases it at least provides reasonable hints for intensity ratios of scalar and quadrupolar components in a spectrum.

V. EXPERIMENTAL RESULTS

Figure 2 gives an overview over the seven permitted two-photon transitions between the $3s^23p^2\,{}^3P_{0,1,2}$ and the $3s^23p4p\,{}^3P_{0,1,2}$ configuration including the nonresonant ionization step across the first IP used for detection. The transitions are arranged according to the two-photon excitation classes discussed above, with cases I and II corresponding to class 1 ($J_\alpha \neq J_\beta$) for either $\Delta J = 2$ or 1, respectively. The transitions labeled III represent class 2 ($J_\alpha = J_\beta = J$ with $J \geqslant 1$), containing scalar and quadrupolar contributions, while case IV corresponds to class 3 ($J_\alpha = J_\beta = J = 0$), which does not exhibit any hyperfine structure. For ^{29}Si, spectra were recorded for all seven transitions, while just the $3s^23p^2\,{}^3P_0 \to 3s^23p4p\,{}^3P_0$ transition without hyperfine splitting, labeled IV, was studied for all stable silicon isotopes to deliver the isotope shift directly.

A. Hyperfine structure of ^{29}Si

Figures 3–5 show the six scans which exhibit ^{29}Si hyperfine splittings, arranged according to the individual cases I, II, and III defined above. Due to the low natural abundance of ^{29}Si of only 4.67% and the rather weak transition probability for

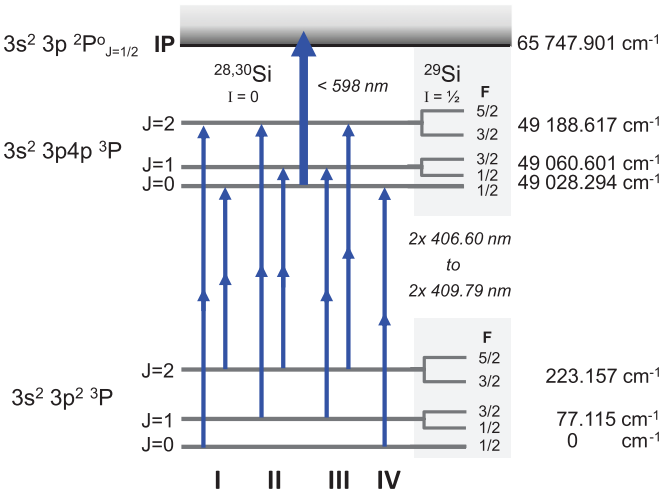

FIG. 2. (Color online) Investigated two-photon transitions in silicon, distinguished into four different cases I, II, III, and IV as discussed in the text.

the two-photon excitation process, the experimental spectra exhibit considerable scattering of data points due to laser and atomic beam fluctuations as well as electronic noise. Generally, an experimental linewidth of about 90 MHz is observed. The value corresponds well to the expectations based on the laser

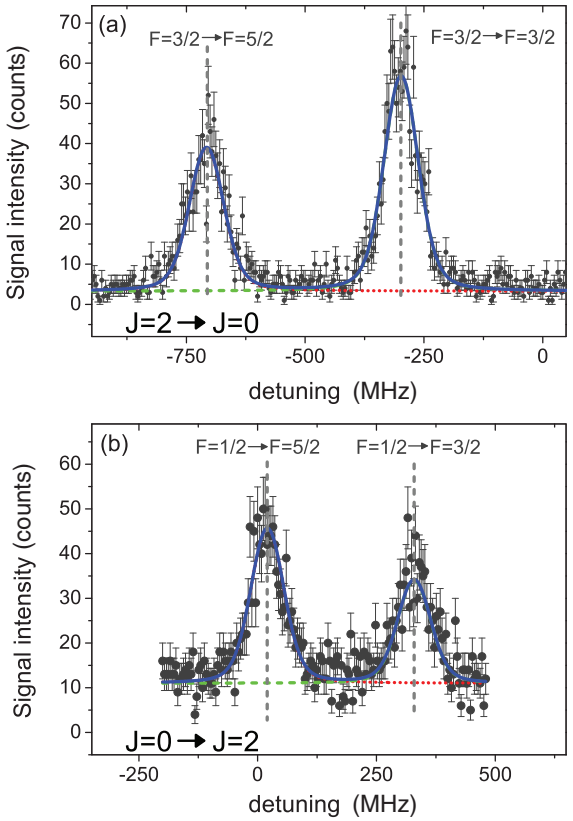

FIG. 3. (Color online) (a) Transition from $3s^2 3p^2\,{}^3P_2 \rightarrow 3s^2 3p4p\,{}^3P_0$ in ^{29}Si. (b) Transition from $3s^2 3p^2\,{}^3P_0 \rightarrow 3s^2 3p4p\,{}^3P_2$ in ^{29}Si. The solid line shows the overall fitted curve, while the dashed and dotted lines show the contribution of the transitions between individual HFS components as labeled.

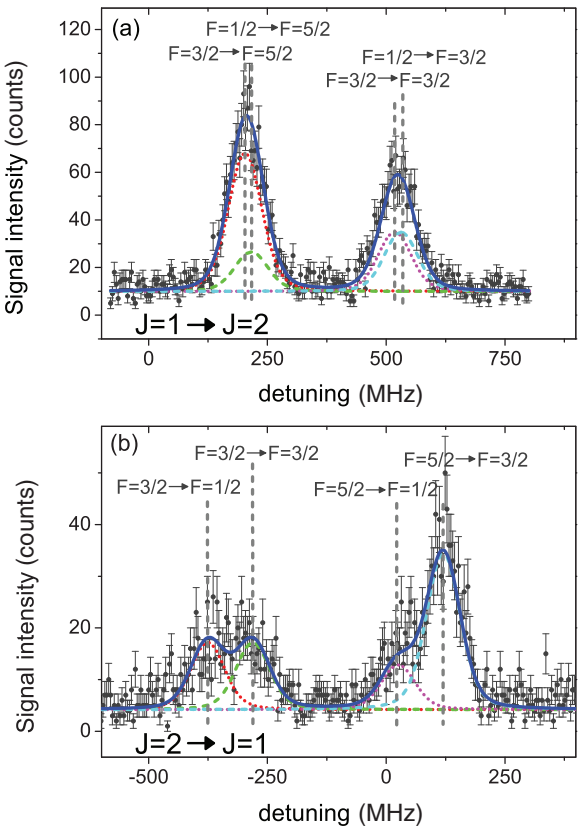

FIG. 4. (Color online) (a) Transition from $3s^2 3p^2\,{}^3P_1 \rightarrow 3s^2 3p4p\,{}^3P_2$ in ^{29}Si. (b) Transition from $3s^2 3p^2\,{}^3P_2 \rightarrow 3s^2 3p4p\,{}^3P_1$ in ^{29}Si. The solid line shows the overall fitted curve, while the dashed and dotted lines show the contribution of the transitions between individual HFS components as labeled.

bandwidth of about 20 MHz of the fundamental laser radiation; the frequency doubling, which necessarily contributes by about a factor of $\sqrt{2}$ to the linewidth; and finally a further factor of 2 stemming from the two-photon process. All diagrams include fit curves to the experimental data. While theoretically the Doppler free part of the two-photon resonance should exhibit a Lorentzian profile, line profiles used for fitting were based on Pseudo-Voigt functions showing a dominant Gaussian contribution ascribed to the laser bandwidth. In addition, as fixed parameters the ratio of peak heights as described by Eq. (9) and identical peak widths were used. These settings reproduced the experimental traces in all cases fairly well.

For case I with $J_\alpha \neq J_\beta$ for $|J_\alpha - J_\beta| = 2$, as shown in Fig. 3, there were two purely quadrupolar transitions with only two well-resolved components. According to the HFS interval rule

$$\Delta E_{F+1} - \Delta E_F = A(F+1), \tag{12}$$

these are simply separated by $\frac{5}{2}$ times the A factor of the corresponding level. Intensity ratios of 2 : 3 are expected from theory, which is well reproduced in the experiment. The values of $A(3s^2 3p^2\,{}^3P_2) = -164(3)$ MHz and $A(3s^2 3p4p\,{}^3P_2) = -124(3)$ MHz are instantaneously extracted from the observed splittings. The ground-state A factor matches the value of $A(3s^2 3p^2\,{}^3P_2) = -160.1(1.3)$ MHz quite well, as measured recently using high-resolution laser spectroscopy [13]. The

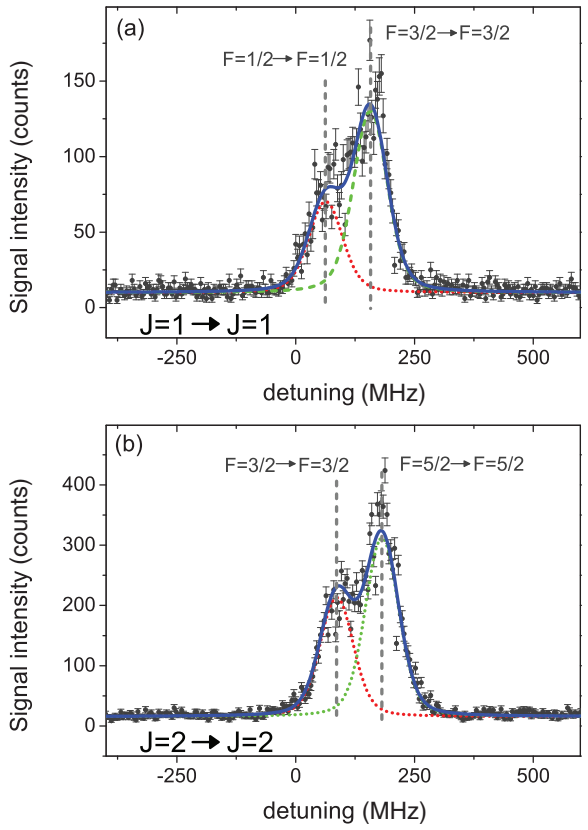

FIG. 5. (Color online) (a) Transition from $3s^2 3p^2\,{}^3P_1 \rightarrow 3s^2 3p4p\,{}^3P_1$ in ^{29}Si. (b) Transition from $3s^2 3p^2\,{}^3P_2 \rightarrow 3s^2 3p4p\,{}^3P_2$ in ^{29}Si. The solid line shows the overall fitted curve, while the dashed and dotted lines show the contribution of the transitions between individual HFS components as labeled.

precision obtained in our study is just a factor of 2 lower. As generally expected the splitting in the higher-lying $3p4p$ level is smaller than the one of the $3p^2$ level, while the observed reduction by just a factor of 1.3 is astonishingly small. This unexpected behavior is ascribed to the fact that the splitting may not dominantly be caused by the valence electron on the highest principal quantum number alone but arises from polarization effects of the whole configuration, which seemingly are similar for both states and thus quite independent of the principal quantum number.

The analysis is well supported by the laser scans in Fig. 4, showing resonances which belong to case II with $|J_\alpha - J_\beta| = 1$. They also show purely quadrupolar two-photon transitions but comprise four hyper-fine-structure components, which are separated by the already determined A factors of the $^3P_2$ state and those of the $^3P_1$ state of either the upper/lower configuration or vice versa. According to classical expectations from ls coupling rules, the splitting of the $J = 1$ states is very narrow. Correspondingly, as this value is on the order of the experimental linewidth for the case of Fig. 4(b) or well below for the case of Fig. 4(a), respectively, in both cases the structures are not resolved. Nevertheless, a fit with fixed intensity ratios, assuming identical widths for all peaks and the necessarily identical distances of the two corresponding peak pairs ($x_1 - x_3 = x_2 - x_4$), provides very good agreement to the experimental data and delivers the splitting with reasonable accuracy. The restriction to identical widths is not perfectly justified, as the different members of the excited-state multiplet decay via different channels and thus might exhibit slightly different total lifetimes. Nevertheless, summing the known transition strength for decays into lower levels from [11], all three upper fine-structure levels result in natural linewidths of about 20 Mhz. In the experiment for none of the transitions a variation of the Lorentzian contribution to the overall linewidths exceeding the error bar was observed. The strong dominance of the Gaussian contribution from the laser in the experimental linewidth was another argument supporting this approach.

Figure 5 shows transitions which should comprise four quadrupolar components plus two scalar components which perfectly overlap two of the others. In contrast to this expectation, only two strongly overlapping components are observed in both cases. This phenomenon is explained in the following way: The $3s3p^3\,{}^5S_2^o$ state located at 33 326 cm^{-1} is considered as the only significantly contributing intermediate state for the two-photon transition probability, as any other candidates of suitable odd parity are located energetically much too far away from the intermediate energy position of 24 500 cm^{-1}. The ratio of scalar and quadrupolar contributions may thus be evaluated using Eq. (9) with a corresponding value for $R(\alpha,\beta;J_r)$ from Eq. (11). In this way, for the case of $J_\alpha = J_\beta = J = 1$, as shown in Fig. 5(a), an intensity ratio of 150 : 1 is computed for scalar to quadrupolar contribution, while for $J_\alpha = J_\beta = J = 2$ [see Fig. 5(b)] a ratio of 60 : 1 is obtained. Correspondingly, only the two scalar transitions with $\Delta F = 0$ were observed, which are separated by the difference of the upper- and lower-state hyperfine splittings. The fit again uses equal widths for each peak and peak height ratios of 1 : 2 or 2 : 3, respectively, calculated with Eq. (9). From Fig. 5(a) a difference in peak position of 97(5) MHz is obtained. The calculated value from the difference in the hyperfine splitting of the respective levels is 75(19) MHz. The discrepancy between the two values, which is just at the error limit, is due to the rather poor signal to noise ratio of the data, in particular for the $J = 1$ hyperfine components. The value for the difference in the peak positions derived from the fit in Fig. 5(b) is 97(3) MHz, this time in good agreement to the value of 99(3) MHz, obtained by subtracting the two values for the hyperfine splitting calculated from the fits in Figs. 3 and 4.

Table I gives an overview of all measured hyperfine splittings of investigated fine-structure levels in ^{29}Si as derived from the fits in Figs. 3 and 4 and the extracted A factors. For a final proof of the extracted hyperfine parameters and to remove the slight discrepancies between the individual results of the overdetermined system of relations we have additionally applied a combined fitting routine jointly considering all data measured in all transitions. This approach used the assignment of hyperfine components as provided unambiguously from the individual fits discussed above and interrelated the spectra via the hyperfine formula with one identical parameter for the hyperfine splitting for each fine-structure level, no matter in which transition it was measured. The results obtained are in perfect agreement with the individual fit results, except for the very narrow splitting of the $3s^2 3p^2\,{}^3P_1$, which is compressed almost to zero by this fitting procedure. The data are more

TABLE I. Observed hyperfine splittings in the investigated fine-structure states in ^{29}Si and A factors as derived by the different approaches discussed in the text.

	$3s^2 3p^2\ ^3P_1$	$3s^2 3p^2\ ^3P_2$	$3s^2 3p4p\ ^3P_1$	$3s^2 3p4p\ ^3P_2$
$F = 0 \rightarrow F = 2$				−311(8) MHz
$F = 2 \rightarrow F = 0$		−410(6) MHz		
$F = 1 \rightarrow F = 2$	37(18) MHz			−308(18) MHz
$F = 2 \rightarrow F = 1$		−400(18) MHz	112(25) MHz	
Weighted mean	37(18) MHz	−409(6) MHz	112(25) MHz	−310(8) MHz
Combined fit	13(16) MHz	−403(3) MHz	95(11) MHz	−314(4) MHz
A factor	8(10) MHz	−163(2) MHz	68(4) MHz	−123(2) MHz
A factor lit. [13]		−160.1(1.3) MHz		

precise due to the larger number of data points entering and due to the stronger boundary conditions for the joint overdetermined fit. We have thus used them to derive the conclusive hyperfine A factors as given.

B. Isotope shift

The isotope shift was determined in the $3s^2 3p^2\ ^3P_0$ to the state $3s^2 3p4p\ ^3P_0$ transition, which does not exhibit a hyperfine splitting for ^{29}Si. Figure 6 compares three scans across the transition for the isotopes ^{28}Si, ^{29}Si, and ^{30}Si. Note the enhancement of the peak intensities for the two weaker isotopes ^{29}Si and ^{30}Si for better visualization.

The three peaks again exhibit a full Gaussian width of about 90 MHz. The background corrected peak heights show a ratio of ^{28}Si : ^{29}Si : ^{30}Si = 92.0% : 4.5% : 3.5% which represents well the natural abundances of 92.23% : 4.67% : 3.10%. Results for the transition isotope shift were extracted from Voigt fit curves as given in Table II. The latter value is in perfect agreement to the expectation for a $^3P_0$ to $^3P_0$, as obtained from the detailed work of Hoover and Holmes [12]. They studied the isotope shift between ^{28}Si and ^{30}Si for all possible single-photon transitions between the $3s^2 3p^2\ ^3P$ to the $3s^2 3p4s\ ^3P$ multiplet and found values between 318(15) and 348(6) MHz with lowest results for low J in both levels involved. In contrast, shifts of up to a factor of 10 or higher were observed by them and confirmed by Lee and Fairbanks, Jr. [13], when a D level was involved. The consistency of the measured isotope shift value for ^{29}Si may be checked by assuming the predicted strong dominance of the mass effect. A value of $\delta\nu_{29,28} = 157(4)$ MHz is obtained as a pure mass shift contribution from $\delta\nu_{30,28}$ and the ratio of the atomic masses for ^{29}Si and ^{30}Si versus ^{28}Si. While in [13] this approach led to a slight underestimation of about 1% of their experimental value, we find an overestimation of about 6%, which slightly exceeds the experimental error bar. Both deviations are ascribed to a small contribution of a field effect, which is opposite for the $P \rightarrow P$ transition as studied here compared to the $P \rightarrow D$ transition investigated by [13]. Due to the small size of this effect, still much higher optical resolution and precision would be required for a quantitative analysis of this trend.

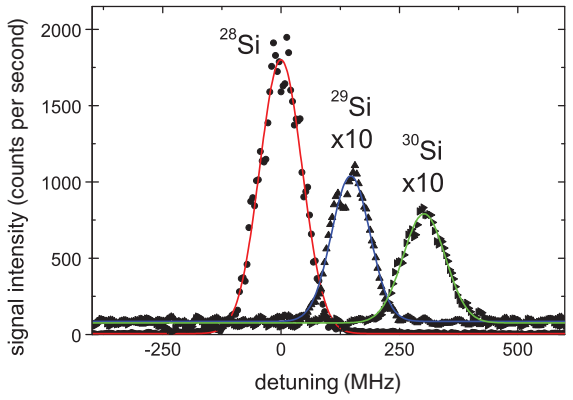

FIG. 6. (Color online) Measured spectra of the $^3P_0 \rightarrow {}^3P_0$ two-photon transition for the isotopes ^{28,29,30}Si. The signal of ^{29,30}Si is enhanced for better visualization. Gaussian profiles are fitted to extract the isotope shifts.

VI. CONCLUSION

Feasibility of a Doppler free two-photon resonance ionization spectroscopy directly inside a hot cavity environment of a resonance ionization laser ion source (RILIS) was demonstrated using an injection-locked narrow-bandwidth high repetition rate pulsed laser. The isotope shift and all hyperfine structures of the transitions between the $3s^2 3p^2\ ^3P_{0,1,2}$ and $3s^2 3p4p\ ^3P_{0,1,2}$ in silicon were recorded at a laser repetition rate of 7 kHz and with an experimental linewidth well below 100 MHz. Hyper-fine-structure parameters as well as isotope shifts could be extracted with a precision of better than 10 MHz. The measured A factor data for the $3s^2 3p^2\ ^3P_2$ level are in good agreement with another recent high-resolution measurement [13], while the measured isotope shifts approve existing expectations for $P \rightarrow P$ levels and thus confirm the very small size of the field effect in this low-mass region. In this study a number of experimental conditions significantly reduced the overall efficiency: the hot cavity was open on two sides, an inefficient nonresonant ionization step was applied, and finally the laser power was still very weak. For application of the technique to studies of exotic

TABLE II. Isotope shift in the $3s^2 3p^2\ ^3P_0$ to $3s^2 3p4p\ ^3P_0$ two-photon transition.

Isotope	^{28}Si	^{29}Si	^{30}Si
This work	0	148(3) MHz	303(7) MHz

species these limitations will be removed as far as possible. To adopt this high-resolution technique a narrow bandwidth high repetition rate Ti:sapphire laser somewhat upgraded in power to the one used here is presently installed at the RILIS of ISOLDE/CERN. A modified on-line ion source and target unit, as proposed initially by Barzakh *et al*. [22] and Denisov [23], is under development too. This comprises a built-in radiation- and temperature-resistant molybdenum mirror in a cavity geometry closed at the rear end, which should be suitable to enable efficient two-photon excitation under the harsh radiation, temperature, and contamination conditions of an on-line isotope separator ion source. Furthermore, the concept shall be applied in combination with the laser ion source trap developed at ISOLDE for isobar suppression in laser ionized exotic nuclides [24] allowing for isomer selection and highest isobar suppression. In conclusion, this new method will allow for direct high-resolution in-source laser spectroscopy on nuclides with both rather low production rates and short half-lives, avoiding any transfer to subsequent experiments and related decay losses during ionization and investigation.

ACKNOWLEDGMENTS

This research has been financially supported by the Deutsche Bundesministerium für Bildung und Forschung under Contract No. 06MZ215 and the Japanese Ministry of Education, Culture, Sports, Science, and Technology Grant-in-Aid for Young Scientists (B) Grant No. 20760592.

[1] Y. Blumenfeld, T. Nilsson, and P. Van Duppen, Phys. Scr. **T152**, 014023 (2013).
[2] R. Catherall, V. Fedosseev, U. Köster, J. Lettry, G. Suberlucq, B. Marsh, and E. Tengborn, Rev. Sci. Instrum. **75**, 1614 (2004).
[3] P. Bricault, F. Ames, T. Achtzehn, M. Dombsky, F. Labrecque, J. Lassen, J.-P. Lavoie, and N. Lecesne, Rev. Sci. Instrum. **79**, 02A908 (2008).
[4] C. Geppert, Nucl. Instrum. Meth. B **266**, 4354 (2008).
[5] V. N. Fedosseev, Y. Kudryavtsev, and V. I. Mishin, Phys. Scr. **85**, 058104 (2012).
[6] V. Fedosseev, D. Fedorov, R. Horn, G. Huber, U. Köster, J. Lassen, V. Mishin, M. Seliverstov, L. Weissman, and K. Wendt, Nucl. Instrum. Meth. B **204**, 353 (2003).
[7] G. Alkhazov *et al*., Nucl. Instrum. Meth. B **69**, 517 (1992).
[8] A. E. Barzakh, I. Y. Chubukov, D. V. Fedorov, V. N. Panteleev, M. D. Seliverstov, and Y. M. Volkov, Phys. Rev. C **61**, 034304 (2000).
[9] L. Weissman *et al*., Phys. Rev. C **65**, 024315 (2002).
[10] U. Köster *et al*., Nucl. Instrum. Meth. B **160**, 528 (2000).
[11] A. Kramida, Y. Ralchenko, J. Reader, and NIST ASD Team, http://physics.nist.gov/asd, accessed 15 July 2013.
[12] J. R. Holmes and M. E. Hoover, J. Opt. Soc. Am. **52**, 247 (1962).
[13] S. A. Lee and W. M. Fairbank, Jr., Phys. Rev. A **82**, 042515 (2010).
[14] C. Mattolat, S. Rothe, F. Schwellnus, T. Gottwald, S. Raeder, and K. Wendt, AIP Conf. Proc. **1104**, 114 (2009).
[15] T. Kessler, H. Tomita, C. Mattolat, S. Raeder, and K. Wendt, Laser Phys. **18**, 842 (2008).
[16] H. Tomita, C. Mattolat, T. Kessler, S. Raeder, F. Schwellnus, K. D. A. Wendt, K. Watanabe, and T. Iguichi, J. Nucl. Sci. Technol. **6**, 37 (2008).
[17] M. Göppert-Mayer, Ann. Phys. **401**, 273 (1931).
[18] L. S. Vasilenko, V. P. Chebotaev, and A. V. Shishaev, Pis'ma Zh. Eksp. Teor. Fiz. **12**, 161 (1970) [JETP Lett. **12**, 113 (1970)].
[19] G. Grynberg and B. Cagnac, Rep. Prog. Phys. **40**, 791 (1977).
[20] U. Fano, Rev. Mod. Phys. **29**, 74 (1957).
[21] B. Cagnac, G. Grynberg, and F. Biraben, J. Phys. (Paris) **34**, 845 (1973).
[22] A. Barzakh, V. Denisov, D. Fedorov, S. Orlov, and M. Seliverstov, Nucl. Instrum. Meth. B **126**, 85 (1997).
[23] V. Denisov, Nucl. Instrum. Meth. A **345**, 99 (1994).
[24] D. A. Fink, S. D. Richter, B. Bastin, K. Blaum, R. Catherall, T. E. Cocolios, D. V. Fedorov, V. N. Fedosseev, K. T. Flanagan, L. Ghys, A. Gottberg, N. Imai, T. Kron, N. Lecesne, K. M. Lynch, B. A. Marsh, T. M. Mendonca, D. Pauwels, E. Rapisarda, J. P. Ramos, R. E. Rossel, S. Rothe, M. D. Seliverstov, M. Sjödin, T. Stora, C. Van Beveren, and K. D. A. Wendt, Nucl. Instrum. Meth. B (2003), doi: 10.1016/j.nimb.2013.06.039.